SUPPLEMENTAL MATERIAL

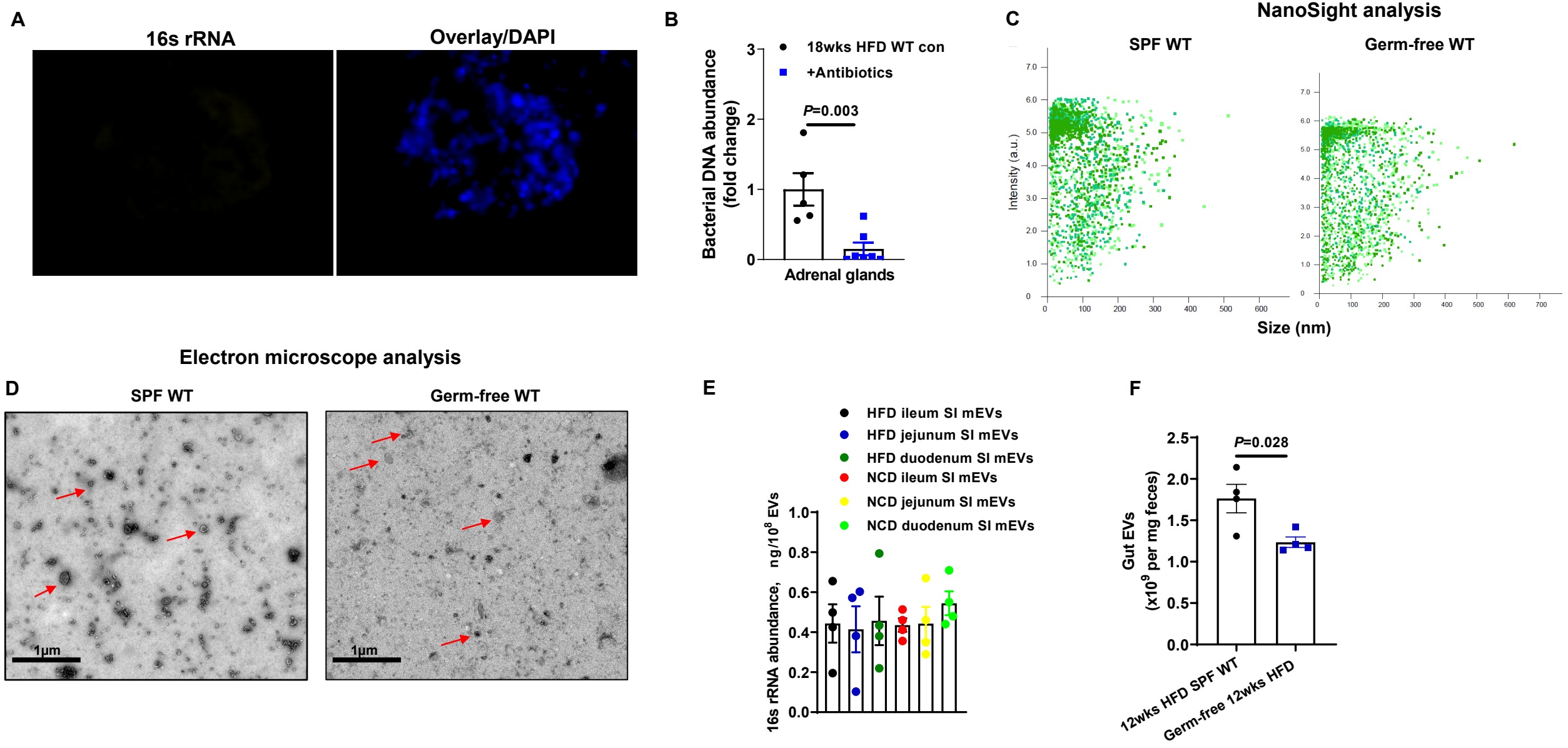

Figure S1. Characteristics of gut mEVs collected from 16wks HFD WT mice, related to Figure 1. A, The existence of 16s rRNA in the pancreatic tissue of 16wks HFD germ-free mice. Data are the representative of three experiments. B, Bacterial DNA abundance in adrenal glands of obese mice after 2 weeks antibiotics treatment. C, The particle sizes of gut EVs were measured by NanoSight analysis. D, The morphology of gut EVs examined by electron microscopy analysis. Red arrows indicate extracellular vesicles. E, qPCR analysis of 16s rRNA levels in the EVs isolated from small intestinal (SI) lumen of lean WT or 16wks HFD WT mice. F, The production of EVs yielded from small intestinal gut lumen contents. NCD, normal chow diet; HFD, high fat diet. SPF, specific-pathogen free. Data are presented as mean ± SEM. *P* values are determined by unpaired two-side Student's *t*-test (B and F).

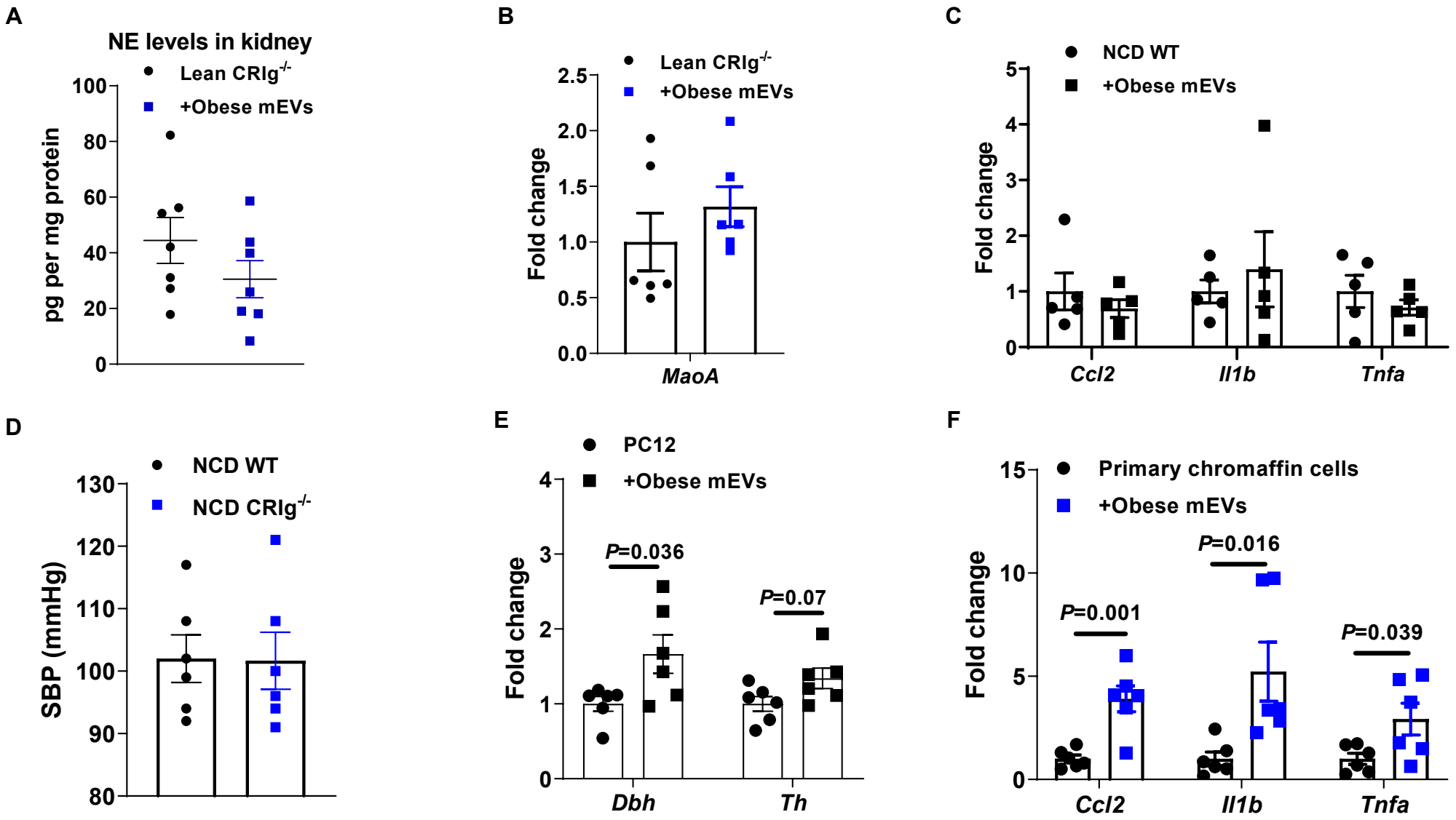

Figure S2. Effects of obese gut mEVs on lean WT mice, related to Figure 2. Norepinephrine (NE) levels in the kidney (A) and monoamine oxidase abundance in adrenal glands (B) of lean CRIg$^{-/-}$ mice after 4 weeks treatment with gut mEVs. C, qPCR analysis of proinflammatory genes in the adrenal glands of lean WT mice after 4wks treatment with obese mEVs. D, The levels of systolic blood pressure (SBP) of lean WT and CRIg$^{-/-}$ mice. E, The abundance of genes associated with catecholamine synthesis in PC12 cells after 24 hours treatment with obese mEVs. F, Effects of gut mEVs on proinflammatory gene expression in primary chromaffin cells isolated from lean WT mice. Data are presented as mean ± SEM. *P* values are determined by unpaired two-side Student's *t*-test (E and F).

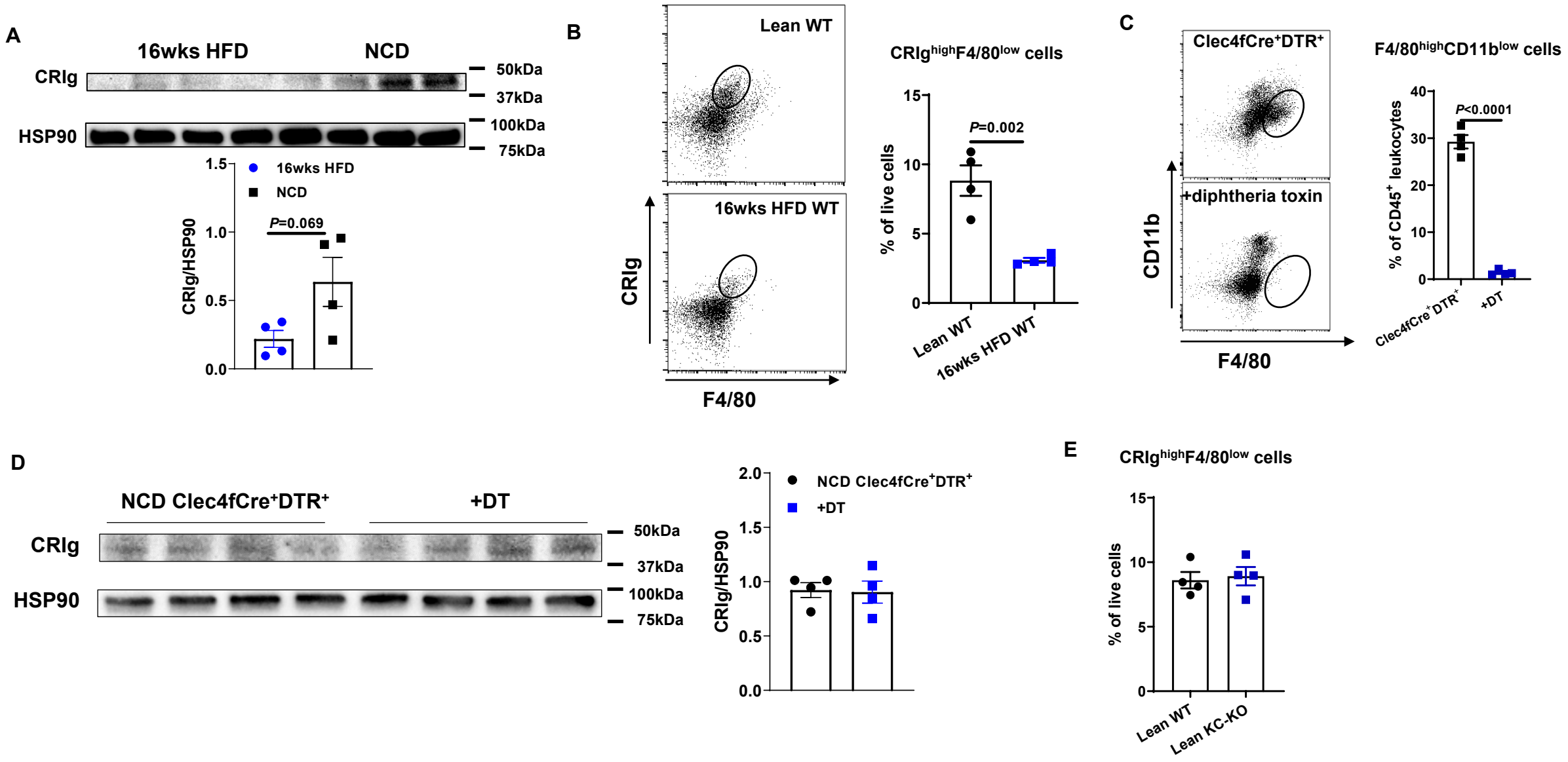

Figure S3. The important roles of adrenal CRIg+ macrophages, related to Figure 3. A and B, Effect of obesity on CRIg abundance in adrenal glands. C, Validation of Kupffer cell ($CD11b^{low}F4/80^{high}$) depletion after lean $Clec4fCre^{+}DTR^{+}$ mice injected with diphtheria toxin (DT) (KC-KO). D, Effect of DT treatment on CRIg abundance in adrenal glands of lean $Clec4fCre^{+}DTR^{+}$ mice. E, Flow cytometry analysis of CRIg+F4/80+ cells in adrenal glands of lean WT and KC-KO mice. Data are presented as mean ± SEM. *P* values are determined by unpaired two-side Student's *t*-test (A-C).

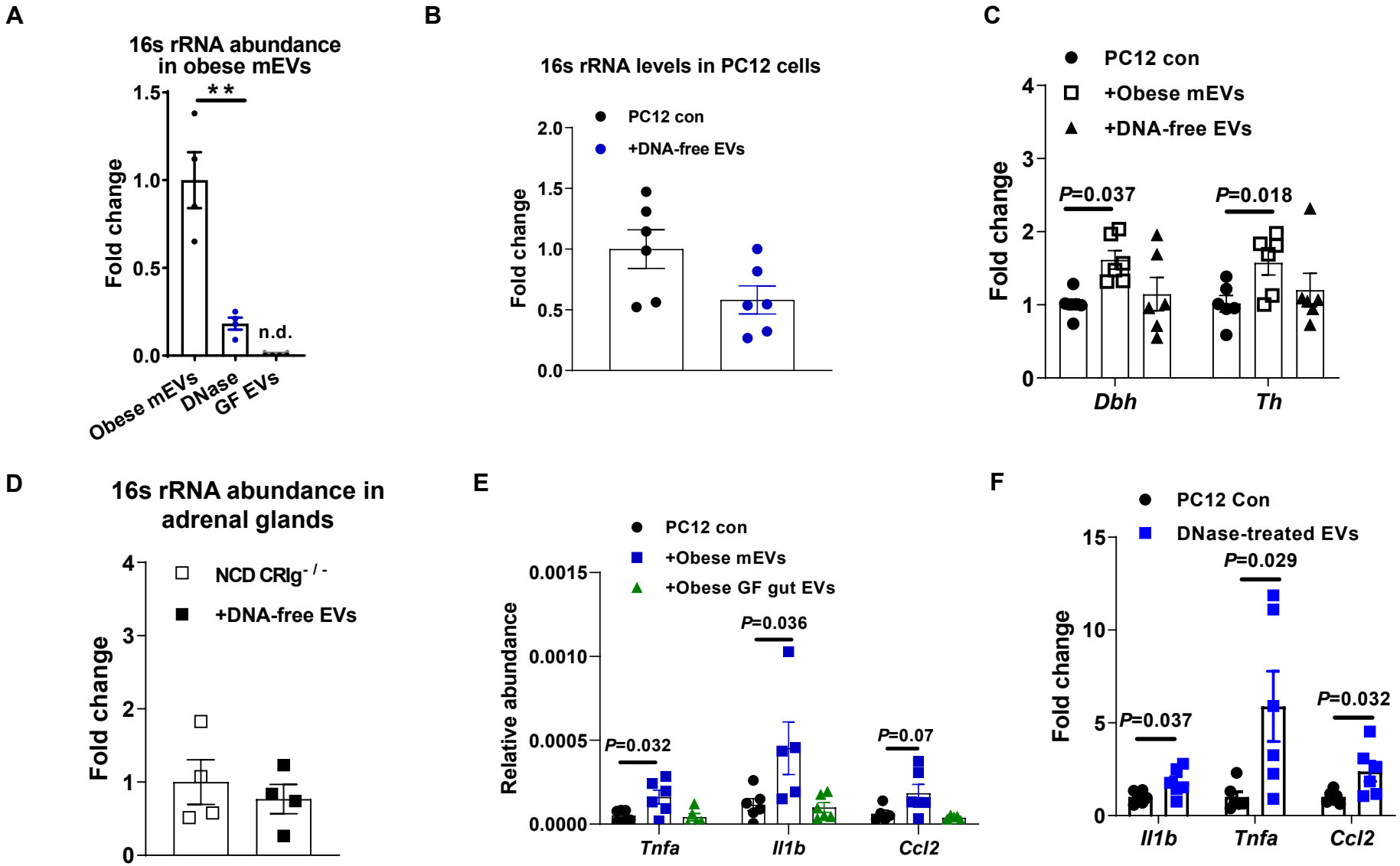

Figure S4. The importance of microbial DNA cargos, related to Figure 4. A, qPCR analysis of 16s rRNA abundance within gut EVs after treatment with electroporation and DNase or gut EVs collected from germ-free mice. n.d. non-detectable. 16s rRNA abundance in PC12 cells (B) or the adrenal glands of NCD CRIg$^{-/-}$ (D) mice after treatment with DNA-free EVs. C, The abundance of key genes associated with catecholamine synthesis in PC12 cells after treatment with either obese mEVs or DNA-free EVs. E, Effects of germ-free gut EVs (GF gut EVs) on PC12 cell inflammation. F, Effects of DNase-treated obese gut mEVs (without electroporation) on PC12 inflammation. Data are presented as mean ± SEM. *P* values are determined by unpaired two-side Student's *t*-test (A and F) or one-way ANOVA (C and E).

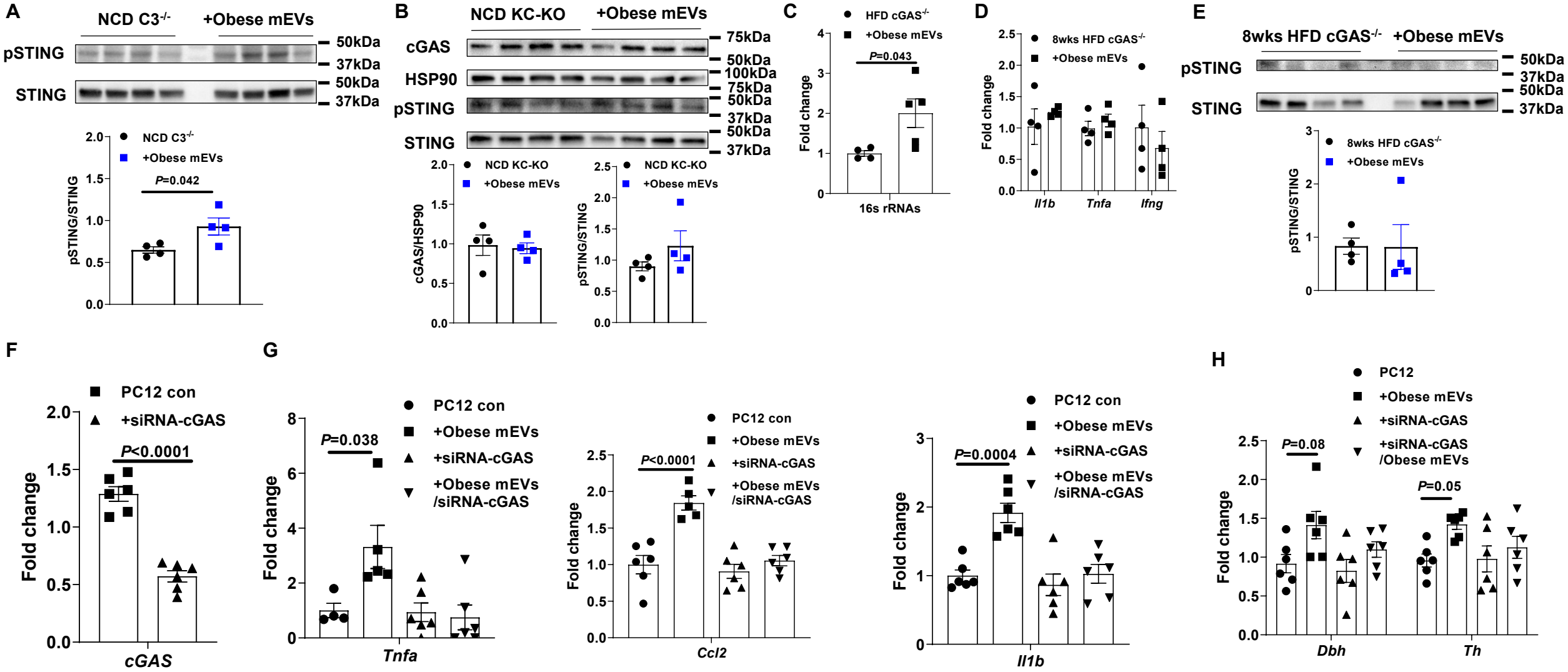

Figure S5. The importance of cGAS/STING activation for the effects of mEVs, related to Figure 5. After 4wks treatment with obese mEVs, the abundance of cGAS/STING in adrenal glands of lean C3$^{-/-}$ (A) or KC-KO (B) mice. C, qPCR analysis of 16s rRNA abundance in adrenal glands after HFD cGAS$^{-/-}$ mice treated with obese mEVs. The abundance of proinflammatory cytokines (D) and activation of cGAS/STING (E) in adrenal glands of HFD cGAS$^{-/-}$ mice after 4wks treatment with obese mEVs. F, Validation of cGAS knockdown in PC12 cells after treatment with siRNA-cGAS for 24 hours. The expression of proinflammatory genes (G) and genes associated with catecholamine synthesis (H) in PC12 cells after treatment with obese mEVs and/or siRNA-cGAS. Data are presented as mean ± SEM. *P* values are determined by unpaired two-side Student's *t*-test (A and F) or one-way ANOVA (G and H).

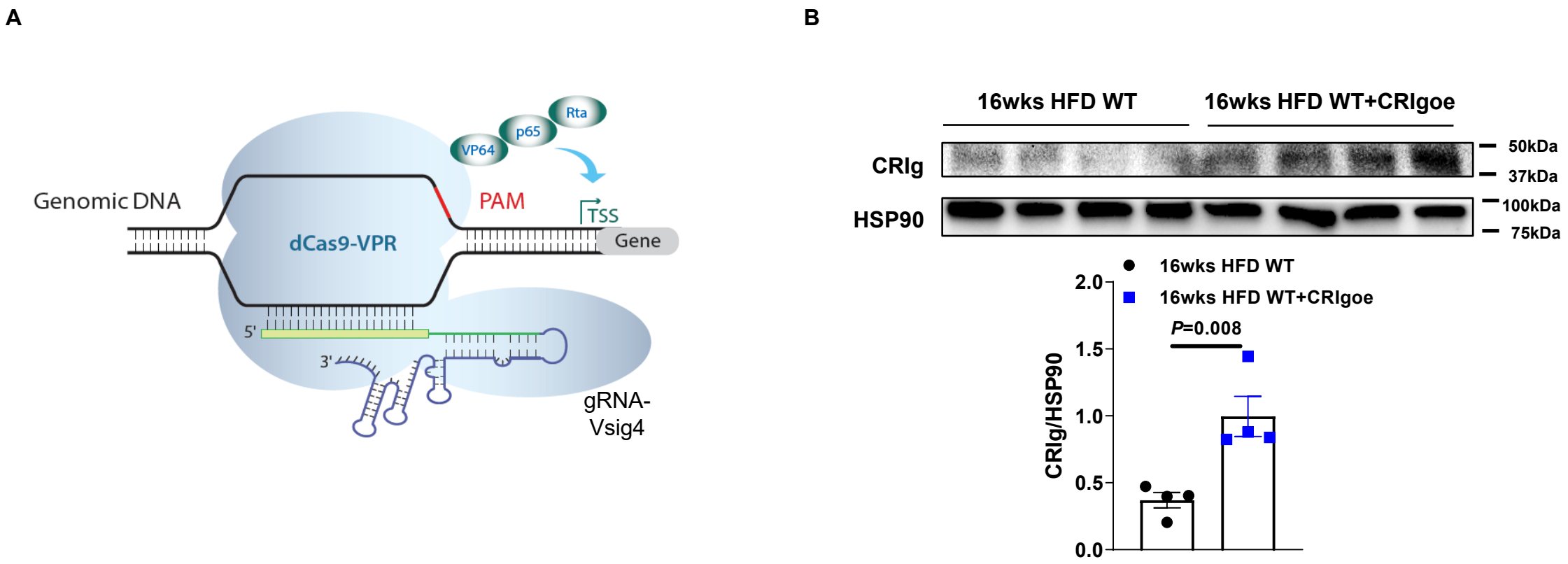

Figure S6. Recovery of Vsig4 gene expression by using the deactivated Cas9-VPR/gRNA system, related to Figure 6. A, The diagram of dCas9-VPR complex targeting Vsig4 gene's promoter region with guide RNA-Vsig4. B, CRIg abundance in adrenal glands of 16wks HFD WT mice after 4wks treatment with lentivirus carrying dCas9-VPR and gRNA-Vsig4. Data are presented as mean ± SEM. *P* value is determined by unpaired two-side Student's *t*-test (B).